INSTITUTE OF PHYSICS PUBLISHING BIOINSPIRATION & BIOMIMETICS

Bioinsp. Biomim. **1** (2006) R1–R16 doi:10.1088/1748-3182/1/1/R01

TOPICAL REVIEW

Micro-optical artificial compound eyes

J W Duparré and F C Wippermann

Fraunhofer Institute for Applied Optics and Precision Engineering, A Einstein Str. 7, 07745 Jena, Germany

E-mail: Jacques.Duparre@iof.fraunhofer.de

Received 28 November 2005
Accepted for publication 16 February 2006
Published 6 April 2006
Online at stacks.iop.org/BB/1/R1

Abstract

Natural compound eyes combine small eye volumes with a large field of view at the cost of comparatively low spatial resolution. For small invertebrates such as flies or moths, compound eyes are the perfectly adapted solution to obtaining sufficient visual information about their environment without overloading their brains with the necessary image processing. However, to date little effort has been made to adopt this principle in optics. Classical imaging always had its archetype in natural single aperture eyes which, for example, human vision is based on. But a high-resolution image is not always required. Often the focus is on very compact, robust and cheap vision systems. The main question is consequently: what is the better approach for extremely miniaturized imaging systems—just scaling of classical lens designs or being inspired by alternative imaging principles evolved by nature in the case of small insects? In this paper, it is shown that such optical systems can be achieved using state-of-the-art micro-optics technology. This enables the generation of highly precise and uniform microlens arrays and their accurate alignment to the subsequent optics-, spacing- and optoelectronics structures. The results are thin, simple and monolithic imaging devices with a high accuracy of photolithography. Two different artificial compound eye concepts for compact vision systems have been investigated in detail: the artificial apposition compound eye and the cluster eye. Novel optical design methods and characterization tools were developed to allow the layout and experimental testing of the planar micro-optical imaging systems, which were fabricated for the first time by micro-optics technology. The artificial apposition compound eye can be considered as a simple imaging optical sensor while the cluster eye is capable of becoming a valid alternative to classical bulk objectives but is much more complex than the first system.

1. Introduction

Miniaturized digital cameras and optical sensors are important features for next-generation customer products. Key specifications are resolution, sensitivity, power consumption, manufacturing and packaging costs and, increasingly important, overall thickness. Digital micro-cameras which are based on miniaturized classical lens designs used today are rarely smaller than $5 \times 5 \times 5\ \mathrm{mm}^3$. The magnification is related to the system length. Recent improvements of CMOS image sensors would allow further miniaturization. Nevertheless, as a result of diffraction effects, a simple miniaturization of known classical imaging optics would drastically reduce the resolution [1] and potentially also the sensitivity. A simple scaling of the imaging system to the desired size does not seem to be a clever approach. How then to overcome these limitations of optics? A fascinating approach is to look how nature has successfully solved similar problems in the case of very small creatures [2].

During the last century, the optical performance of natural compound eyes has been analyzed exhaustively with respect to resolution and sensitivity [3]. Several technical realizations or concepts of imaging optical sensors based on the principle of image transfer through separated channels have been presented in the last decade. However, since the major challenge for a technical adoption of natural compound eyes consists of the

 © 2006 IOP Publishing Ltd Printed in the UK

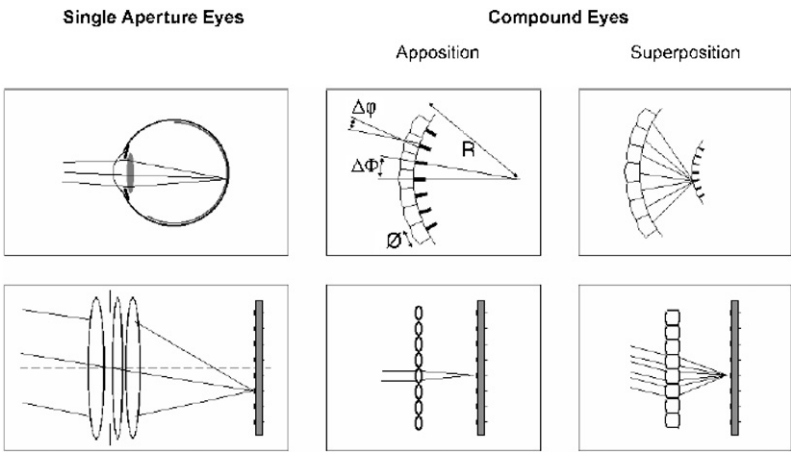

Figure 1. Different types of natural eye sensors (top) and their technical counterparts (bottom) [2].

required fabrication and assembly accuracy, all those attempts have not led to a breakthrough because classical, macroscopic technologies have been exploited to manufacture microscopic structures. Sometimes only schematic macroscopic devices have been fabricated. It is the aim of this paper to show that these limitations can be overcome by using state-of-the-art micro-optics technology. Many imaging applications could benefit from bioinspired micro-optics, in a way that classical objectives never could. Compound eye cameras should, for instance, fit into tight spaces in automotive engineering, credit cards, stickers, sheets or displays, security and surveillance, medical technology and not be recognized as cameras.

Section 2 provides an introduction into natural compound eye vision, which is necessary to understand and classify the presented work on artificial compound eyes. Furthermore, an introduction into micro-optics principles and scaling laws of imaging systems is given. The state-of-the-art of micro-optical imaging systems which have their archetypes in natural compound eyes is presented in the context of the corresponding natural vision principle.

In sections 3 and 4, two different objectives on the basis of artificial compound eyes are examined. In the apposition optics (section 3), a microlens array is applied with a photodetector array of different pitch (center distance between two adjacent elements) in its focal plane. The image reconstruction is based on Moiré magnification [4]. The cluster eye approach (section 4), which is based on the superposition of compound eyes, produces a regular image. Here three microlens arrays of different pitches form arrays of Keplerian microtelescopes with tilted optical axes, including a field lens. The two artificial compound eye concepts provide a decoupling of magnification and system length. Furthermore, the use of individual channels for each viewing direction in artificial compound eyes allows a channelwise correction of off-axis aberrations, for instance, using chirped anamorphic microlenses. Both types of objectives are analyzed with respect to the theoretical limitations of resolution, spatial information capacity, sensitivity and system thickness. Explicit design rules and possibilities for simulation are derived. The different fabricated systems are experimentally characterized with respect to resolution and sensitivity.

Finally, section 5 concludes the results of the presented work and points out future tasks with respect to design, adaption to applications and technologies, in order to develop bioinspired micro-optical vision systems from the proof of principle to commercial applications.

2. Natural vision

Natural compound eyes have been subject to scientific research for more than a century. This section only covers the essential basics of natural compound eye vision. For further reading, [3] and [5] are especially recommended.

There exist two known types of animal eyes [6]: single aperture eyes and compound eyes. The latter can be further divided into apposition compound eyes and superposition compound eyes (figure 1). All of these eye types can use refractive mechanisms for image formation while incorporating graded refractive index optics [7]. In single aperture eyes and superposition compound eyes, reflective mechanisms can be found as well [8, 9].

For small invertebrates with an external skeleton, eyes are very expensive in weight and metabolic energy consumption. If the budget is tight, nature prefers to distribute the image capturing to a matrix of several small eye sensors instead of using a single eye [3, 5]. The resolution of compound eyes is usually poor compared to that of single aperture eyes [10]. But the processing of highly resolved images would overload the brain of small insects anyway. In nature, this lack of resolution is often counterbalanced by a large field of view (FOV) and additional functionality such as polarization sensitivity or fast movement detection. The arrangement of optical channels on a spherical shell allows compound eyes to have a large FOV while the total volume consumption remains small. Hence, the main volume of the head is still available for the brain and signal processing.

2.1. Single aperture eye

The key advantages of single aperture eyes (figure 1, left column, top row) are high sensitivity and resolution. The

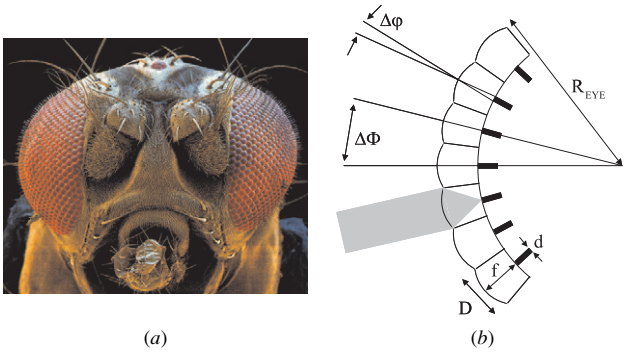

(*a*) (*b*)

Figure 2. Natural apposition compound eye. (*a*) Head of the fruit fly '*Drosophila melanogaster*'. (*b*) Operation principle of natural apposition compound eyes: apposition compound eyes are composed of hundreds up to tens of thousands of microlens–receptor units referred to as ommatidia arranged on a curved surface with radius R_{EYE}. Every microlens with diameter and pitch D and focal length f focuses light only from a small solid angle $\Delta\varphi$ of object space onto a small group of photoreceptors. For simplicity, one receptor with diameter d is assumed per unit. The eye samples the angular object space with the interommatidial angle $\Delta\Phi$. D and R_{EYE} determine the size of $\Delta\Phi$. The ommatidia are optically isolated by intermediate opaque walls to prevent crosstalk. The arrangement of ommatidia on a spherical shell allows natural apposition compound eyes to have a very large FOV while the total volume consumption is small.

small size of the FOV and the large volume of single aperture eyes constitute drawbacks. Furthermore, as single aperture eyes image only a limited FOV sharply, they must be moved to sample the entire visual surrounding. This is accomplished by means of eye or head movement. In addition, processing the large amount of visual information in a highly resolved image requires a large brain. Since this is a scientifically well-covered topic, this natural vision system is not discussed in more detail in this introduction.

2.2. Apposition compound eye

A natural apposition compound eye consists of an array of microlenses on a curved surface. Each microlens is associated with a small group of photoreceptors in its focal plane. Apposition compound eyes have mainly evolved in diurnal insects such as flies (figure 2(*a*)) [11]. The single microlens–receptor unit forms one optical channel and is commonly referred to as an ommatidium. The term 'microlens' is convenient and further used for referring to the focusing element. In fact, however, the principal focusing element of the ommatidium is the crystalline cone, which has a graded refractive index, with the highest index on the optical axis. Only a minor contribution to the focusing is provided by the corneal lens [7, 12].

Pigments form opaque walls between adjacent ommatidia to avoid, in the case of large angles of incidence (AOI), light which is focused by one microlens being received by an adjacent channel's receptor. Otherwise ghost images and a reduction of contrast would result.

Natural apposition compound eyes contain several hundreds (water fly) up to tens of thousands (honeybee or Japanese dragon fly) of these ommatidia packed in non-uniform hexagonal arrays. Each ommatidium's optical axis points in a different direction in the object space (figure 2(*b*)). For simplicity, only one photoreceptor is assumed per unit. The visual surrounding of the insect is sampled with the interommatidial angle

$$\Delta\Phi = D/R_{\mathrm{EYE}}. \tag{1}$$

A response in the corresponding photoreceptor results only if an object point is located on the optical axis of an ommatidium, or close to it. The image formation evolves by the contribution of all ommatidia's signals.

The size of the so-called acceptance angle $\Delta\varphi$ defines, according to the Sparrow criterion [13], the minimum distance of two bright point sources which can still be resolved by the optics. $\Delta\varphi$ has a geometrical contribution $\Delta\rho = d/f$ which is determined by the receptor diameter projected into the object space. This is convolved with a contribution given by diffraction at the microlens aperture [14] for the wavelength λ, resulting in

$$\Delta\varphi = \sqrt{\left(\frac{d}{f}\right)^2 + \left(\frac{\lambda}{D}\right)^2}. \tag{2}$$

Here a Gaussian photoreceptor response is assumed. λ/D is the full width half maximum (FWHM) of the Gaussian approximation of the Airy function describing the blur caused by diffraction [15].

How does the resolution of a compound eye scale with size? Using the formalism of the eye parameter [14], it can be shown that

$$R_{\mathrm{EYE}}\Delta\Phi^2 \geqslant \lambda/2, \tag{3}$$

and furthermore by substituting $\nu_s = 1/(2\Delta\Phi)$ (the Nyquist frequency), it follows that

$$R_{\mathrm{EYE}} \geqslant 2\lambda\nu_s^2. \tag{4}$$

The eye radius is proportional to the square of the required resolution. In contrast, in single aperture eyes this scaling is linear. The problem arises because, in compound eyes, the ommatidia must increase in both number and size in order to increase resolution [16]. The eyes become too large or reveal, for the same size, a much lower resolution than single aperture eyes ('A man would need a compound eye of at least 1 m diameter to get the same angular resolution as with his lens eye.' [17]).

This is the reason why many invertebrates developed compound eyes which have areas with a locally higher resolution, 'acute zones', than elsewhere in the eye. These acute zones point into the direction of highest interest, similar to the fovea in the eyes of mammals [18, 19].

Various technical approaches for compact vision systems adopted the principle of small apposition compound eyes. A general examination of the properties of natural apposition compound eyes and of the possibilities of using artificial derivates of those was given in [20]. Graded index microlens arrays (MLA) of the rod type in front of pinhole arrays and photodiode arrays built up an artificial apposition compound eye [21]. Here a bulk diverging lens was used to provide the overall FOV. The overall image reconstruction is explained by

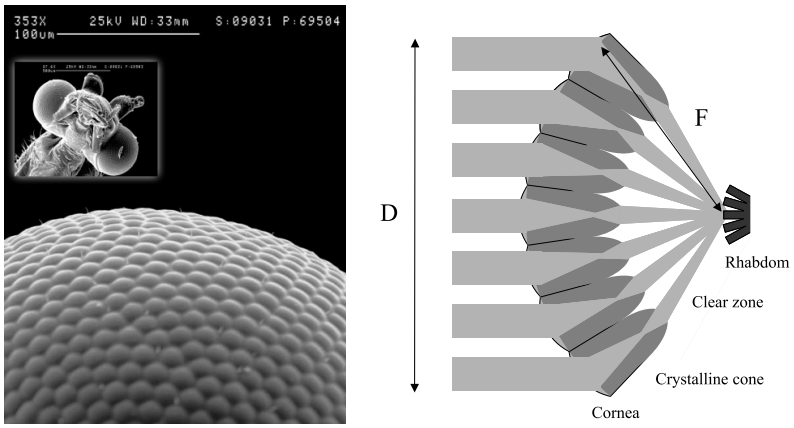

(*a*) (*b*)

Figure 3. Natural superposition compound eye. (*a*) Scanning electron microscope image of head and eye section of the moth '*Ephestia Kuehniella*'. (*b*) Schematic cross section of natural superposition compound eye.

the Moiré magnification. A detector geometry with a large pitch and low fill factor (ratio of optically sensitive area to unit cell area) has to be applied in order to achieve a high resolution with the Moiré-image reconstruction. Different arrangements of graded index microlenses and pinholes in the cells of the array allow scale-invariant processing. A difference in pitch leads to a factor of magnification which can also be interpreted as enlargement of the FOV [22]. In this approach, the number of image points is in general equal to the number of ommatidia. This results in a drawback of the systems described in the literature because here the number of ommatidia is very small. The same applies to other attempts where, for instance, microelectromechanical systems (MEMS) technology is used. A scanning retina for a change of direction of view was realized [23]. An autonomous navigating robot was developed using an array of elementary motion detectors based on a macroscopic artificial apposition compound eye objective in a radial arrangement [24]. In the TOMBO system [25], only a small number of channels are used, but each cell of the system has a matrix of associated photoreceptors which pick up all the information of the micro-images. The microlenses are centered with the matrix of photodetectors capturing the micro-images. The difference in the micro-images is the result of the different radial positions of the corresponding channel within the array (slightly different offset). For close objects, the information content of the overall image calculated from all the micro-images is much larger than that of the single micro-images. However, there is the burden of extraordinarily complex image processing [26].

Latest developments in this field deserve a special mention [27]. Artificial compound eyes have been developed using a novel three-dimensional (3D) microfabrication method. Combining polymer microlenses, reconfigurable microtemplating, soft lithography and self-written waveguides by self-aligned 3D photo-polymerization enables a spherical arrangement with thousands of omni-directional self-aligned microlens and waveguide arrays in a photo-sensitive polymer resin. This work also offers a promising paradigm for constructing miniaturized optical systems for omni-directional detection, wide FOV or fast motion detection [28]. However, to date, to the authors knowledge actually captured images using these approaches have not been demonstrated yet.

2.3. Superposition compound eye

The natural superposition compound eye has primarily evolved in nocturnal insects and deep water crustaceans (figure 3). The light from multiple facets combines on the surface of the photoreceptor layer to form a single erect image of the object [6]. For the refractive type, this optical performance is not the result of a single MLA layer but of an array of microtelescopes. These microtelescopes also incorporate graded index lenses [29]. Compared to natural apposition compound eyes, natural superposition compound eyes are much more light sensitive. Eyes with small $F/\#$ (stop or aperture number, ratio of focal length and aperture diameter, often referred to as 'speed' of the lens, since the smaller this number is, the shorter the necessary exposure time), even smaller than 1, have been observed. Aberrations—similar to spherical aberrations, but caused by the combination of light from many facets—lead to a resolution far from the diffraction limit [30]. Some insects use a combination of both types of compound eyes. Variable pigments switch between apposition (daylight) and superposition (night) or change the number of recruited facets making up the superposition image [31].

The planar technical equivalent of the refractive natural superposition compound eye is the Gabor superlens [32]. A Gabor superlens is formed by two MLAs of different pitches, having infinite conjugates. The two confocal MLAs build up an array of beam steering miniature telescopes. The pitch difference of the two MLAs introduces a continuous displacement of the microlenses in the second array, bending all bundles toward a common focus [33].

A large variety of imaging applications and manufacturing methods were proposed for this lens [34]. The closest technical application of the refractive natural superposition compound eye can probably be found in highly symmetric one-to-one

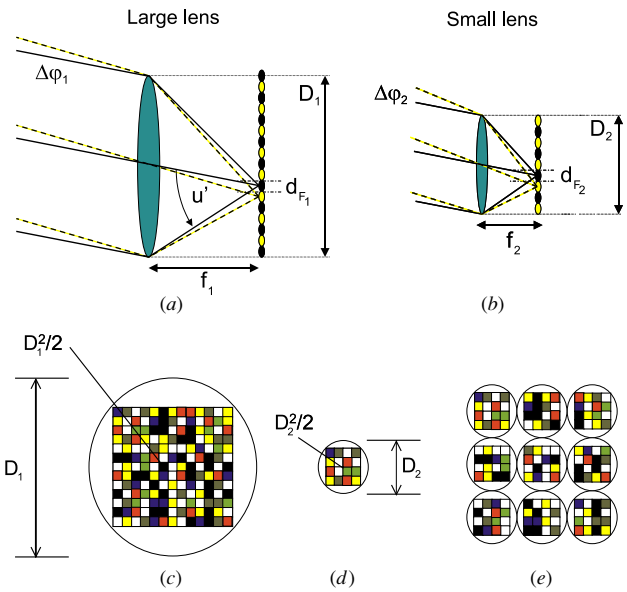

Figure 4. Scaling of lenses with constant $F/\#$ [2]. (*a*) Large lens. The size of one image point is given by 2.44 λ $F/\#$, where λ is the wavelength. As a result of the large focal length f_1 the angular projection of the Airy disc in the object space $\Delta\varphi_1$ is very small. The lens system has a high angular resolution. (*b*) Small lens. The size of the Airy disc is the same as in (*a*). However, due to the short focal length f_2, here the angular projection of the Airy disc in the object space $\Delta\varphi_2$ is very large. The lens system has a low angular resolution. (*c*) The amount of information in the image plane of a large lens is very large, because of the small Airy disc and large focal length resulting in a large image field. (*d*) Even if the size of the image points is the same, the spatial information capacity of the small lens is low because of the small image field. Only a few image points can be resolved. (*e*) By applying an array of microlenses (*d*), which separately transfer the information in parallel, the same information capacity as with the bulk lens in (*c*) can be achieved.

imaging systems as, for instance, in photocopying machines using graded index MLAs [35]. In photocopying machines, numerous channels of the overall array contribute to the formation of one image point in order to achieve a high light gathering power [36]. The microlens photolithography [37] applies a highly symmetric one-to-one telescope imaging system. A photolithographic mask is transferred into photoresist with homogeneous image quality over an 8 inch wafer diameter with only millimeter working distance and a large focal depth.

2.4. Scaling laws of imaging systems

In micro-optics, aberrations are not as critical as in bulk optics, as for instance third-order spherical aberration scales linearly with the lens diameter. For small scale lens systems, the diffraction limit itself is the important criterion describing resolution and image finesse. This limitation can be avoided by using MLAs and parallel information transfer instead of single microlenses.

The spatial size of the diffraction-limited point spread function (PSF), d_F, in the lenses focal plane is invariant when scaling with constant $F/\#$. The angular projection of d_F into object space, however, increases with miniaturization (figures 4(*a*) and (*b*)). Scaling with constant $F/\#$ also means the maintenance of FOV. Fewer angular sensitivity functions fit in the lenses' FOV, and the amount of transferred information is decreased.

Most of the described technological approaches of artificial compound eyes for compact vision systems suffer from assembly misalignment errors of the individually fabricated components. This has prevented the realization of functional thin cameras with a large number of pixels. Macroscopic technologies have been explored in order to realize microscopic devices.

As a consequence of the small required lens sags artificial compound eyes are well suited for micro-optical fabrication technologies. These allow wafer level manufacturing of compound eye objectives with a large number of channels. Utilizing photolithographic processes results in a highly precise lateral accuracy of the compact imaging systems. Fabrication and assembly technologies on a wafer scale lead to cheap and compact imaging devices because of the parallel manufacturing of many systems at once.

3. Artificial apposition compound eye objective

Artificial receptor arrays such as CCD or CMOS sensors are fabricated on planar wafers. Thus, a thin monolithic objective based on the artificial compound eye concept has to be a planar structure as well. The artificial apposition compound eye consists of an MLA positioned on a substrate, preferably with optical isolation of the channels, and an optoelectronic detector array of different pitch in the microlenses' focal plane [38, 39]. The pitch difference enables the different viewing directions of each optical channel. Each channel's optical axis points in a different direction in object space with the optical axes of the channels directed outward (figure 5) if the pitch of the receptor array is smaller than that of the MLA. Consequently, an upright Moiré-magnified image results. If the pitch of the MLA is smaller than that of the receptor array, the image is inverted. A pinhole array can be used to narrow the photosensitive area of the detector pixels if they are not small enough for the required resolution.

A planar artificial apposition compound eye as shown in figure 5 is described by the same optical parameters as its curved natural archetype. Behind each microlens a small image of the object is generated. As a result of the pitch difference between the MLA and pinhole array, $\Delta p = p_L - p_P$, a Moiré-magnified image [40] is obtained when the pinholes have different amounts of offset with respect to the microlenses sample the micro-images [41]. Each channel corresponds to one field angle in object space. The acceptance angle $\Delta\varphi$ determines the tradeoff between sensitivity and resolution. It has to be small in order to have a high resolution and large in order to achieve a high sensitivity. The interommatidial angle of the planar apposition compound eye is

$$\Delta\Phi = \arctan\frac{\Delta p}{f}. \tag{5}$$

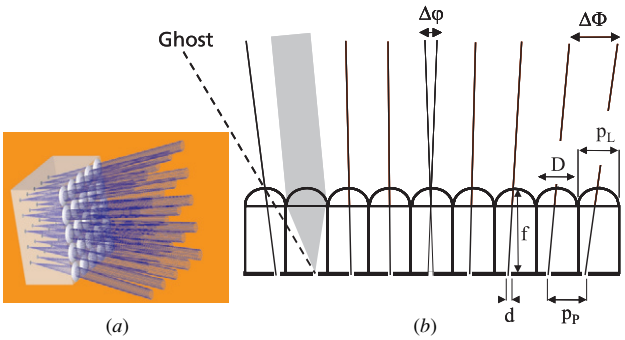

Figure 5. Schematic diagram of a planar artificial apposition compound eye. (*a*) Three-dimensional model of the artificial apposition compound eye showing the focusing MLA, the pinhole array in its focal plane and the tilted optical axes of ommatidia because of a pitch difference between the microlens array and pinhole array, enabling the FOV of the imaging system. (*b*) The thin monolithic device consists of an array of microlenses with diameter D, focal length f and pitch p_L on the front side of a spacing structure and a pinhole array with pinhole diameters d and pitch p_P in the microlenses' focal plane on the spacing structure's backside.

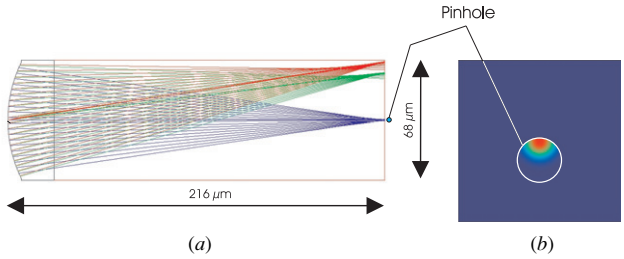

Figure 6. Simulation of a single channel for determination of the angular sensitivity function. (*a*) Diagonal cross section of single ommatidium. Length is 216 μm, $R = 75$ μm, and the microlens is in a UV-curing polymer on a glass substrate. Field angles 0°, 11°, 13.5° are shown. The pinhole is centered on the optical axis. (*b*) Intensity distribution in the pinhole for an incident plane wave at a 0.35° angular offset from the optical axis (pinhole diameter: $d = 2$ μm; position: focal plane of the microlens centered on the optical axis). Consequently, a reduced power is coupled, compared to the on-axis illumination. Simulation method: 'physical optics propagation' in ZEMAX™.

As in the natural equivalent, opaque walls are introduced between ommatidia to prevent the crosstalk of adjacent channels for object points outside the FOV and the resulting ghost images (the oblique ray in figure 5(*b*) demonstrates the ghost effect).

The overall image size of the artificial apposition compound eye is determined by the Moiré magnification $p_P/\Delta p$ and thus completely independent of the system length. This arrangement delivers an image with a much larger magnification than that of a single microlens. But it has a much shorter system length than a classical objective with the same magnification. The magnification, or in other words the equivalent focal length of the artificial apposition compound eye (which is defined by the ratio of lateral Moiré-image size and FOV) determining the magnification, is thus much larger than the overall objective length. This results in a huge telephoto ratio (ratio of focal length to system length) of >100 which in conventional telephoto objectives is only approximately 2–3.

A further advantage of the artificial apposition compound eye is the large focal depth. As a result of the extremely short focal length of the microlenses an object is focused independently of the object distance. There is no need for an active focus adjustment with respect to the object distance.

3.1. Design and simulation of the artificial apposition compound eye

There are two main possibilities for characterization. The first is the examination of the complete array of channels. Here, the interaction of channels to provide one overall Moiré-magnified image can be observed. But there is only a limited number of analysis tools available. However, the image forming capability of the artificial apposition compound eye can be proved this way. Much more information about the objective can be obtained by analyzing the performance of a single ommatidium. Many valuable tools for optical design and analysis are available. The extrapolation from a single ommatidium to an array of channels forming the final artificial apposition compound eye has to be harmonized with the single-channel parameters, but is otherwise comparatively simple.

The angular sensitivity function is the most appropriate method for characterizing the performance of a single ommatidium. It predicts which solid angle in object space is treated by the optical system as one image point. The amount of flux, radiated from an object point which is actually received by a photoreceptor, is plotted as a function of angular distance of the object point from the optical axis of the considered ommatidium. The exact representation is the convolution of the microlens PSF with the pinhole, projected into object space by the focal length of the microlens. The field-dependent angular sensitivity function explicitly includes diffraction, aberrations and pinhole size. It is obtained by using commercially available ray-tracing software.

First, the microlens PSF including aberration effects and diffraction at the microlens aperture is calculated for a certain field angle. It is then multiplied by the transmission function of the pinhole. The angular offset of the considered field angle from the ommatidium's viewing direction determines how much power of the PSF is transmitted by the pinhole (figure 6(*b*)). This procedure is repeated for different amounts of offset of the field angle from the ommatidium's viewing direction. The coupled optical power is plotted as a function of the offset.

Figure 7 shows the simulation of the angular sensitivity function of a later realized system, where the efficiency is normalized to the flux incident on the lens at $\lambda = 0.55$ μm. The artificial apposition compound eye principle shows a clear tradeoff between sensitivity and resolution: the larger the pinhole diameter, the higher the sensitivity but the wider the angular sensitivity function, resulting in lower resolution (overlap of the channel's FOVs) and vice versa [10, 42]. In approximation, the angular sensitivity function has a Gaussian

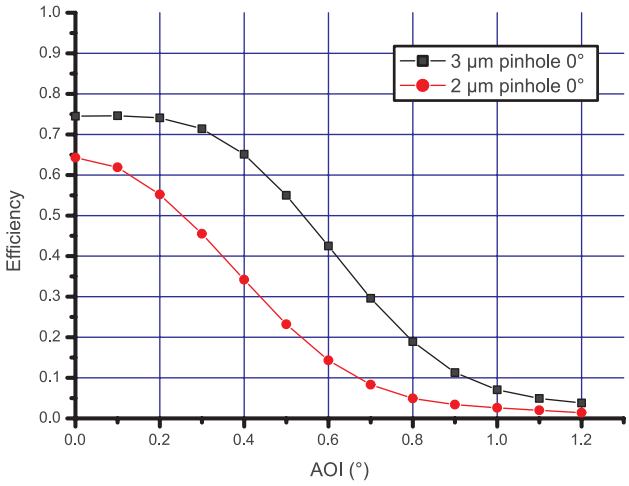

Figure 7. Simulated angular sensitivity function for a single ommatidium with $D = 68$ μm and $f_{n'} = 216$ μm. Two different pinhole sizes are examined for on-axis performance.

shape, if the pinhole and the PSF are of similar size. The pinhole size is then well matched to the PSF in terms of resolution and sensitivity. If the pinhole is larger than the PSF there results in approximation of the angular sensitivity function a super-Gaussian shape, in extreme cases this is close to a rectangular shape. Then, a small change in object position close to the viewing direction is not reflected in any change of the angular sensitivity function. The resolution is low. If the pinhole is smaller than the PSF, the width of the angular sensitivity function is also small, but limited by the size of the PSF. Furthermore the sensitivity is low.

In natural insect eyes, the microlens layer and the light sensitive cells are both arranged on a curved base (figure 2(*b*)). Each optical channel focuses the light coming from the object points lying on the channels' optical axis. Due to bending each ommatidium points toward a different angular direction. Therefore these compound eyes exhibit a very large FOV while the single channels are working on-axis and are not suffering from off-axis aberrations [43]. As mentioned above, to date, artificial apposition compound eye objectives are limited to planar substrates. Consequently, the optical channels cannot be arranged in on-axis configurations inherently connected with the appearance of off-axis aberrations when using spherical lenses. In classical macroscopic optical systems (archetype: single chamber eye), where one optical channel transfers the overall FOV, many optical elements of different refractive indices have to be used in order to minimize off-axis aberrations leading to very complex, bulky and expensive optical systems which only represent a compromise of aberration correction for all viewing directions.

In contrast, for the apposition compound eye objective each lenslet is assigned to only one angle of the overall FOV. Consequently, an individual correction of the channels for aberrations is feasible [43]. Due to the small numerical aperture of the lenslets of the objective, astigmatism and field curvature are by far dominant compared to coma which is only a minor influence. Therefore efficient channelwise focusing of

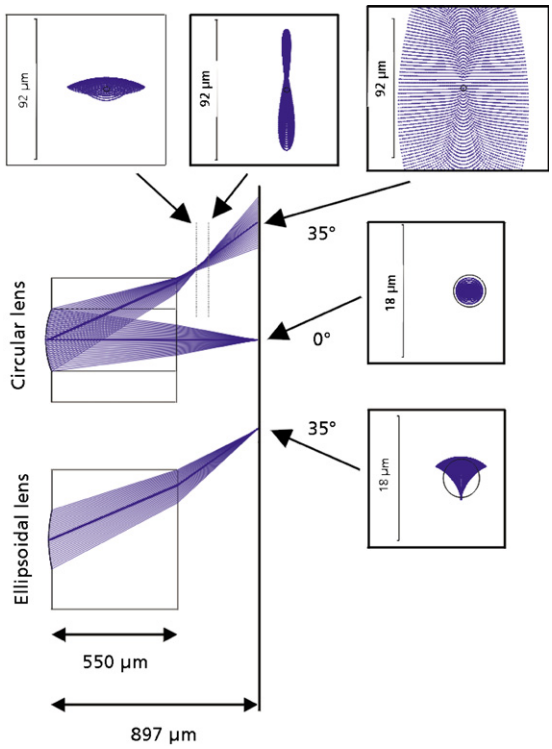

Figure 8. Circular and ellipsoidal lenses under perpendicular and oblique incidence and related spot diagrams (arrows indicate the position of the corresponding spot). A circular lens with a radius of curvature $R = 339$ μm and diameter $D = 242.8$ μm in fused silica ($n = 1.46$ at 550 nm wavelength) under perpendicular incidence produces a diffraction-limited focus. However, if illuminated under oblique incidence, astigmatism and especially field curvature lead to very large spots in the Gaussian image plane. The tangential and sagittal image planes are separated from the Gaussian image plane (here -165 μm and -262 μm, respectively), and the foci are blurred to lines. Using an anamorphic lens with adapted tangential and sagittal radii of curvature ($R_t = 579$ μm, $R_s = 451$ μm) for this special angle of incidence, a diffraction-limited spot size is achieved.

the oblique angle to be transferred is possible by using different and differently oriented anamorphic lenses for each channel [44]. The radii of curvature of the lenses in the two orthogonal directions (tangential and sagittal planes) have to be different and chosen in order to compensate for astigmatism due to the oblique incidence. Furthermore, they are both chosen in such a way that the focal plane of all cells with their different angles of incidence is fixed at the position of the paraxial image plane (figure 8). This leads to a planarized Moiré-magnified image [4, 40, 41] in the detector surface. A torus segment with two radii of curvature in perpendicular directions is the most appropriate 3D surface type for such an anamorphic lens. A channelwise decenter of the lens vertex with respect to the assigned receptor center enables the correction of the distortion of the complete objective.

3.2. Fabrication

The fabrication of the artificial apposition compound eye has been carried out using lithographical processes on a wafer

scale. It is based on the patterning of a thin 4 inch glass wafer with arrays of microlenses in a rectangular arrangement on one side and pinhole arrays on the opposite side. The thickness of the wafer is matched to the microlens focal length in the glass.

The generation of the MLAs consists of several steps involving master and mold generation and subsequent UV-replication [45]. The photoresist master pattern is fabricated on a silicon wafer in a standard procedure (photolithography in combination with a heating/reflow process [46]) since it is a well-established technology yielding very smooth and well-determined spherical surfaces [46] often used for imaging applications [47]. Here the 3D surface is the result of surface tension effects and depends on the volume of the resist cylinder and the shape of the rim of the lens (mask geometry). Consequently stringent limitations of viable geometries apply. A suitable approximation of the desired torus segment is an ellipsoidal lens which can be easily formed by melting a photoresist cylinder on an ellipsoidal base [48]. For the correction of astigmatism and field curvature the ellipses have varying major and minor axes as well as adapted orientations (see the right-hand side of figure 17). To our knowledge, commercially available mask software tools are not capable of generating masks of a chirped arrangement. Therefore self-written software tools had to be developed. The required geometry data for the mask necessary for creating the chirped array of ellipsoidal lenses can be derived completely analytically [49]. The replication is carried out in a modified contact mask aligner (SUSS MA6 with a UV-embossing option) where the gap between the glass wafer and mask/mold is filled by a UV-curing inorganic–organic hybrid polymer which is subsequently cured and separated from the mold. The most critical fabrication issue is the uniformity of the axial distance between the microlens vertex and pinhole, which is affected by a series of parameters such as precision of the MA6-height-alignment (± 1 μm), bowing of the mold, mask holder, chuck and substrate (± 6 μm overall) as well as by non-uniform microlens focal lengths across the wafer (± 3 μm).

An artificial apposition compound eye has a low fill factor of pinholes in the image plane. It is consequently more suitable for optoelectronic sensor arrays which also have a low fill factor rather than for a combination with conventional densely packed CCD or CMOS sensor arrays. Therefore, ultra-thin artificial apposition compound eyes customized to the geometrical parameters of a large-pitch CMOS sensor for low-cost, fast and robust vision, even under extreme illumination conditions [50], were designed and fabricated.

The pitch of the artificial apposition compound eyes pinhole array was matched to the pixel pitch of the sensor array. For given FOV and $F/\#$ a design thickness of 206 μm and a regular MLA pitch of 69.35 μm resulted for the objective. Objective chips with different pinhole sizes covering the photo-sensitive area of the sensor pixels were realized on a wafer scale in order to examine the influence on resolution and sensitivity (figure 9). The wafers were subsequently diced and the objectives were aligned in front of the detector array (figure 10) [51]. Some objectives were fixed to the sensor array by UV-curable glue for permanent use as a thin camera system.

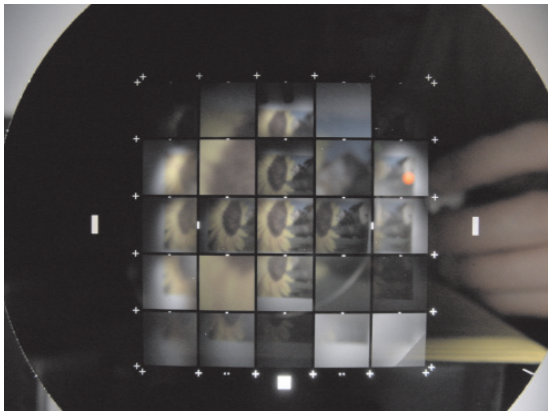

Figure 9. Wafer with 5×5 ultra-thin objectives before singularization, imaging the picture of a sunflower. Objectives with different pinhole sizes and also objectives with equal pitches of the microlens array and pinhole array resulting in unity magnification are realized.

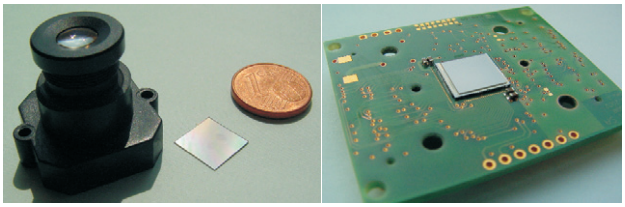

(*a*) (*b*)

Figure 10. Diced artificial apposition compound eye. (*a*) Artificial apposition compound eye in comparison to 1 Euro cent and a traditional single lens objective with the same magnification and approximate length of 20 mm. (*b*) Artificial apposition compound eye attached to the CMOS sensor array (courtesy of Centre Swiss d'Electronique et de Microtechnique SA (CSEM) Neuchâtel, Switzerland).

The size of the object, presented to the vision system without opaque walls must be matched to its FOV to avoid the crosstalk of adjacent channels. Otherwise, in the case of large AOI from object points outside the FOV in the current setup, light focused by one microlens may be received by a receptor of the adjacent channel. Ghost images from objects outside the FOV and a reduction of contrast may result. In order to overcome this problem, the realization of an artificial apposition compound eye with opaque walls using a high aspect ratio photolithography technology on a supporting substrate was investigated.

The region between pinholes and microlenses is not formed by a simple substrate but by a structured spacer layer consisting of transparent columns of SU8 photo-polymer (EPOXY NOVOLAK EPON SU8) and gaps which are filled by absorbing polymer cast. The patterning of the columns was realized by SU8 resist technology using an additional photomask (figure 11(*a*)). After hard baking of the SU8 columns the gaps were filled by highly absorbing polymer cast (PSK2000 black matrix polymer, Brewer science) as shown in figure 11(*b*). Pinhole and microlens fabrication remains unchanged. Finally, the MLA was replicated on top of this spacing structure (figure 11(*c*)). The sum of

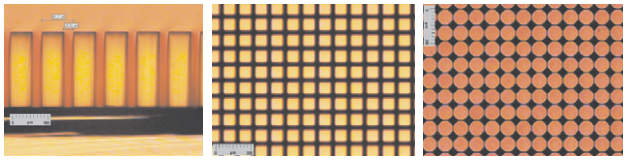

(*a*) (*b*) (*c*)

Figure 11. Photographs of fabrication of opaque walls. (*a*) Side view of transparent columns of photo-polymer which are structured with a high aspect ratio in SU8, forming the bulk structure of the channels. (*b*) Gaps are filled by light-absorbing polymer cast (front view). (*c*) MLA is replicated on top (front view).

SU8 thickness and replicated thickness was uniform to within $\pm 1\%$. In future this procedure could be applied directly to the optoelectronics wafer as a supporting substrate. This enables the integration of the objective assembly in the electronics fabrication process. However, at the current stage of development a direct integration of this fabricated objective including opaque walls on top of the imager was not possible due to the required thickness of the supporting glass substrate.

3.3. Experiments

The artificial apposition compound eye is aligned actively in front of the sensor array using a vacuum gripper arm which is attached to a precision six-axis manipulation stage. The sensor board is fixed to a rotation stage with the rotation axis in the center of the detector array. A homogeneous white target is presented to the camera. The artificial apposition compound eye and the sensor board are aligned with respect to each other until all the pinholes are centered on their corresponding detector pixels and a homogeneous bright image is obtained from the sensor. Rotation between the objective and sensor is especially critical and has to be avoided. Different test patterns were presented to the vision system composed of the thin artificial apposition compound eye and the 'artificial retina' optoelectronic sensor array. The captured images are analyzed with respect to resolution and sensitivity, focusing homogeneity and subjective information content. The size of the object presented to the vision system had to be matched to its FOV to avoid crosstalk of adjacent channels due to the lack of opaque walls between the channels in a version directly applicable to the imager.

A radial star pattern is well suited to determine the optical cut-off frequency of an imaging system. Here the object frequency is a function of the radial coordinate in the image. The resolution in LP/degree (LP stands for 'line pair' and is a measure of resolution) is estimated by the cut-off of resolution in the image of the radial star pattern centered within the objective's FOV.

Figures 12(*a*) and 13(*a*) show images of the same star pattern taken using the artificial apposition compound eye in figure 12(*a*) and using a bulk, 1/3 inch image-format objective in figure 13(*a*). Figure 13(*a*) demonstrates the limitation of resolution by the sensors' Nyquist frequency. The artificial apposition compound eye achieves approximately half that resolution (figure 12(*a*)). For an artificial apposition

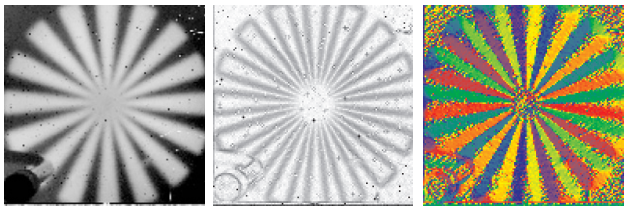

(*a*) (*b*) (*c*)

Figure 12. Radial star pattern with 16LP filling the FOV of the 0.2 mm thin artificial apposition compound eye with $d = 2$ μm pinholes. A cut-off resolution at 32LP/FOV can be determined resulting in a resolution of 3.6 LP mm^{-1} or 1.5 LP/degree and a FOV of $20^\circ \times 20^\circ$. The black and white dots are due to random data transmission errors of the sensor's ethernet communication with the PC. The vacuum gripper for holding the objective over the sensor array appears in the lower left corner of the captured test images. (*a*) Intensity image. (*b*) Close-to-the-pixel analogous computation of contrast. (*c*) Edge orientation (false color coded).

(*a*) (*b*) (*c*)

Figure 13. Test images using a bulk objective for comparison (a) and captured by the artificial apposition compound eye (b), (c). (*a*) The same test pattern as in figure 12 was also recorded using a bulk objective for 1/3 inch image format with a focal length of 12 mm and an $F/\#$ of 2.0. In this case, the resolution is limited by the sensor's Nyquist frequency to 64 LP/FOV. (*b*) Image of a portrait photograph of Carl Zeiss. (*c*) Example of imaged bar targets for MTF determination (here 16 LP bar target).

compound eye with $d = 2$ μm pinholes, a cut-off resolution of 32 LP/FOV was determined. The capabilities of the optoelectronic sensor array with a low fill factor are presented in figures 12(*b*) and (*c*). It suits not only the acquisition of intensity images but, due to the low fill factor, especially the close-to-the-pixel on-chip analogous computation of contrast and contrast direction without post-processing in a subsequent computer.

Figure 13(*b*) shows the caption of a portrait photograph of Carl Zeiss using the artificial apposition compound eye. This demonstrates the capability of face recognition.

Bar targets of different spatial frequencies, such as in figure 13(*c*), were imaged for a quantitative MTF determination. Each signal frequency response (SFR) was calculated by a FFT formalism where the amplitude of the first harmonic with respect to the dc peak of the original and the imaged bar patterns are compared and plotted versus the corresponding angular frequency in figure 14. The measured MTF for $d = 2$ μm pinholes corresponds to the cut-off predicted by the image of the radial star pattern in figure 12(*a*). Approximately 30 LP can be resolved over the entire FOV. The limiting factor of resolution of the generated artificial apposition compound eye is the overlapping of the acceptance

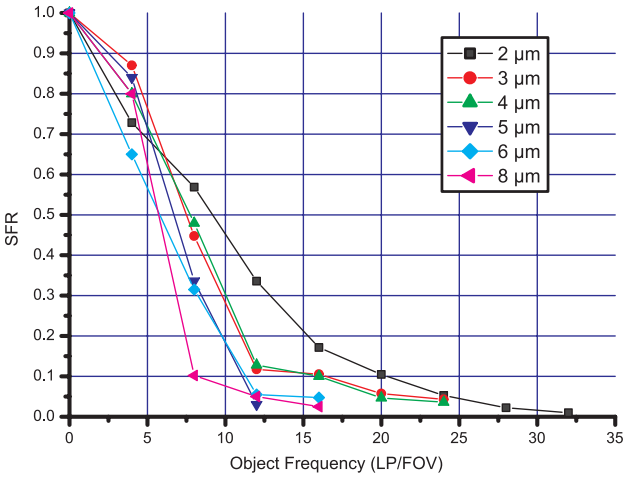

Figure 14. MTF of artificial apposition compound eye with d as the parameter.

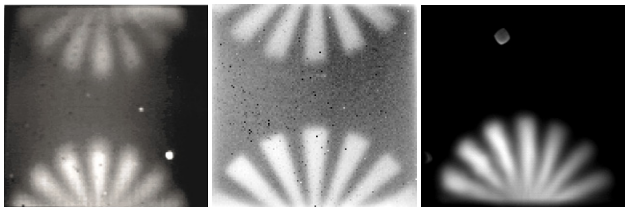

(*a*) (*b*) (*c*)

Figure 15. Original and ghost images with and without opaque walls by imaging a test pattern strongly off-axis. (*a*) Without opaque walls, 101 × 101 channels, $d = 5$ μm pinholes. (*b*) Without opaque walls, 128 × 128 channels, $d = 2$ μm pinholes, directly attached to the sensor. (*c*) With opaque walls, 101 × 101 channels, $d = 5$ μm pinholes. The white dots are mask defects.

Table 1. Measured sensitivity of compound eye camera with $F/\#$ of 2.2 normalized using the bulk objective with the same sensor array and bare pixels.

Pinhole diameter (μm)	2	3	4	5	6	8
Relative sensitivity (%)	2.4	4.8	10.0	15.2	35.0	38.3

angles of adjacent channels in object space which increases with increasing pinhole diameters.

However, using small pinholes for the improvement of resolution results in reduced sensitivity. In table 1 the captured optical powers using artificial apposition compound eyes with different pinhole sizes are normalized to the power using the bulk objective with a sensor array with bare pixels for taking the same plain image.

For evaluation of the crosstalk, the radial star pattern was imaged off-axis by systems without opaque walls (figures 15(*a*) and (*b*)) under the same conditions as by a system including optical isolation between ommatidia (figure 15(*c*)). The radial star pattern is imaged under a large AOI so that half of it is outside the objective's FOV.

For artificial apposition compound eyes without opaque walls, a ghost image of the part of the test pattern which is outside the objective's FOV appears on the opposite side of

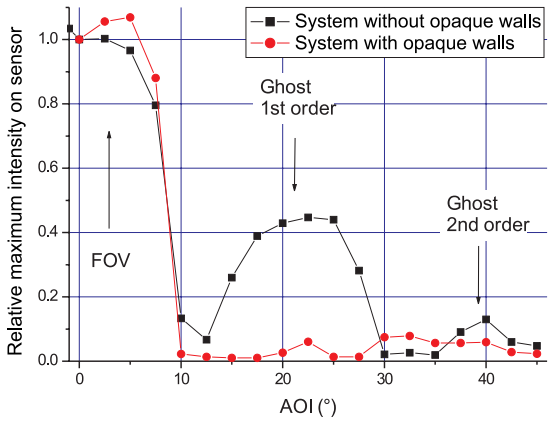

Figure 16. Maximum intensity on the sensor versus AOI. The region of AOI 'FOV' is that with the corresponding microlens focusing on a pinhole. In the angular region of 'ghost first order' the focus of the adjacent microlens is brought on a pinhole and consequently for 'ghost second order' the focus of the next but one microlens.

the image. For the artificial apposition compound eye with opaque walls included in the spacing structure, there results a blocking of light from outside the FOV. Only the original part of the pattern is imaged (figure 15(*c*), compare to figure 15(*a*)). Ghost images are suppressed.

This is confirmed by a quantitative measurement of the response of the artificial apposition compound eyes with and without opaque walls with 101 × 101 channels and $d = 3$ μm pinholes to a 0.65° extended source. The source is presented to the imaging system under different angles of illumination inside and outside the FOV. The wafers with the artificial apposition compound eyes are attached to a rotation stage and tilted in order not to loose light from the transfer through the relay optics for large AOI. The test object, the relay optics and the CCD are fixed. The corresponding diagram for the maximum intensity on the sensor as a function of AOI is given in figure 16.

Figure 16 quantitatively shows the effect of opaque walls on imaging quality. The signal-to-noise ratio (SNR) of the maximum intensity on the sensor is drastically increased. Real image signals can be separated from false light much more easily than without opaque walls. A fully operational ultra-thin imaging device based on artificial apposition compound eye vision even for arbitrary large illuminated scenes is only achieved if opaque walls are introduced between adjacent channels.

For the evaluation of the improved resolution homogeneity by use of chirped ellipsoidal microlens arrays, we displayed different representative test patterns to a vision system consisting of a chirped lens array and, for comparison of the regular lens array, investigated the captured images with respect to resolution homogeneity over the FOV. For simplicity, only one quadrant of the entire symmetrical FOV is tested so that the channel in the lower left corner has a perpendicular viewing direction with respect to the objective plane and consequently applies a circular lens. With increasing viewing angle of the channel, the ellipticity of the

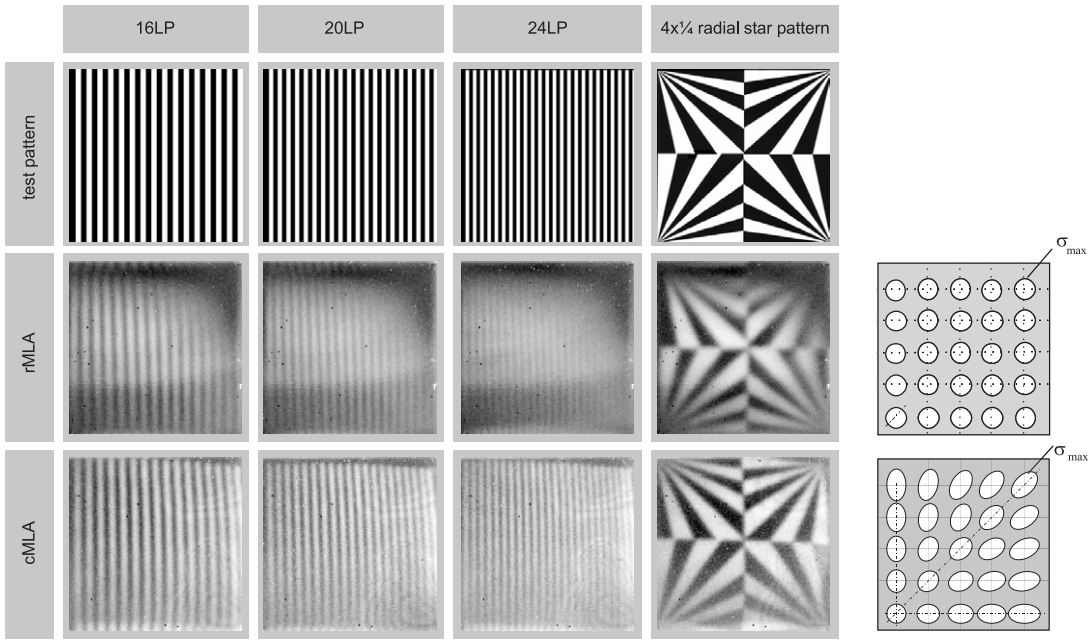

Figure 17. Bar targets of different spatial frequency and captured images of them using a chirped lens array for channelwise aberration correction for the oblique incidence and using a regular lens array for comparison. Additionally, a specially adopted $4 \times 1/4$ radial star test pattern demonstrates the obtainable resolution in the four image corners as a function of the angle of incidence by the different radii of vanishing contrast of the radial star patterns.

corresponding lens is increased up to an angle of $\sigma_{\max} = 32^\circ$ on the diagonal.

Figure 17 shows original bar and radial star test targets and the corresponding images taken by compound eye objectives applying chirped or regular lens arrays. It can be clearly observed that—as to be expected—the resolution in the center of the FOV (the lower left corner of the objective) is independent of the use of regular or chirped lens arrays. However, with an increasing viewing angle the resolution is decreased, however when simply using the regular lens array while the resolution stays constant when applying the chirped lens array where each channel is individually optimized for its viewing direction [52].

4. Cluster eye

Archetypes for this micro-optical telescope compound eye imaging system (we will call it a 'cluster eye') are natural superposition compound eyes of small nocturnal insects. The cluster eye imaging system has basically the same arrangement of lenses as a Gabor superlens to allow for the optical annexation of the micro-images transferred by the different channels (figure 18). The parallel transfer of different parts of an overall FOV (different information) with strong demagnification by separated optical channels allows the cluster eye to have a collective space bandwidth product which is equal to the sum of the individual channel's space bandwidth products. Consequently, the cluster eye has the potential for much higher resolution than the experimentally demonstrated artificial apposition compound eye. On the other hand, the complexity of the cluster eye is much higher

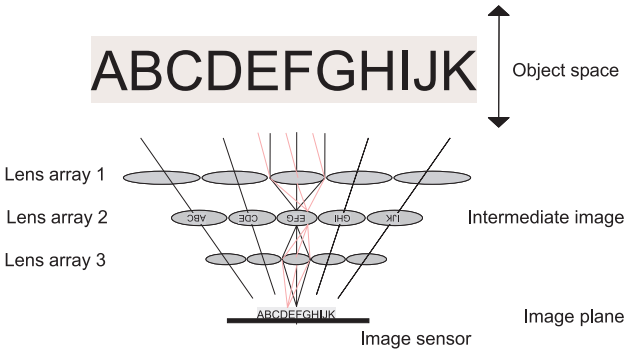

Figure 18. Working principle of the telescope compound eye imaging system with optical image reconstruction. The arrangement of the refracting surfaces is similar to that of a Gabor superlens (natural archetype: superposition compound eye) in order to achieve the image annexation. Field apertures in the intermediate image plane avoid overlay of the images of the different channels to reduce aberrations. For simplicity, only the central chief rays from the different object points are drawn, except for the central channel, where the marginal rays are also shown for two different object directions.

as compared with the artificial apposition compound eye objective, and the cluster eye is thicker by a factor of 10. Three wafers of microlens arrays with applied aperture arrays have to be stacked precisely, and there is a high demand on the microlens quality with respect to focal length accuracy. Other advantages of using artificial compound eye imaging systems apply in the same way for the cluster eye as they do for the artificial apposition compound eye. Such advantages are the manufacturing of the objective by micro-optics technology due

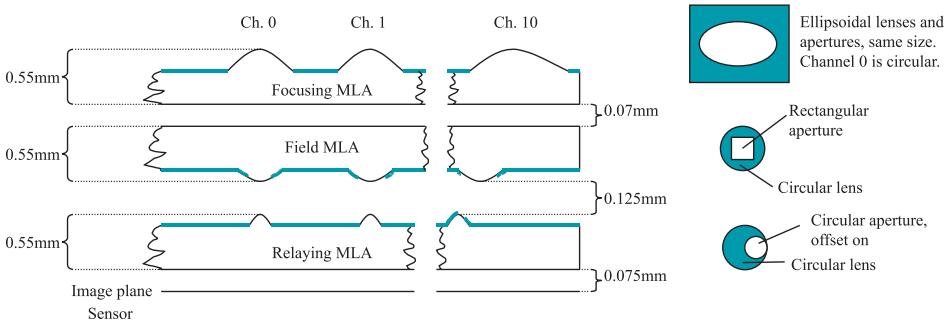

Figure 19. Schematic of the experimentally realized cluster eye. The focusing MLA includes ellipsoidal microlenses. The field MLA and the relaying MLA consist of circular microlenses. Chromium apertures are attached to all MLAs. Rectangular field apertures on the field lenses allow a spatial annexation of the partial images to one regular image. The design's total thickness is 1.92 mm.

to the small required lens sags and correction of each channel for its central viewing direction.

4.1. Principle and design

Figure 18 presents the optical system with no overlap of the images transferred by different channels but a perfect spatial annexation to the upright overall image in the detector surface. Three MLAs with different pitches form Keplerian telescopes with tilted optical axes including a field lens array and field aperture array in the intermediate image plane. The arrangement of the refracting surfaces is similar to that of a Gabor superlens (natural archetype: superposition compound eye). The system can be interpreted as a cluster of single pupil micro-cameras which have tilted optical axes to obtain a large overall FOV [53]. Each channel images only a small angular section. The widths and positions of the field apertures determine the amount of overlap and spatial annexation of the partial images. The ratio of focal lengths of the telescope lenses and tilt of the optical axes of the telescopes determine the magnification and image annexation.

A full description of such a system has to be based on an analytical model to find all reasonable parameter sets and the fundamental relationships. In [54, 55] the determination and validation of the first-order parameters of a cluster eye in the one-dimensional case using a paraxial 3×3 matrix formalism is reported. The obtained paraxial parameters are transferred to parameters of real microlenses. A 2 mm thin imaging system with 21×3 channels, $70^\circ\times 10^\circ$ FOV and $4.5\times 0.5\,\mathrm{mm}^2$ image size is then optimized using sequential ray-tracing. Non-sequential ray-tracing analysis is used for the evaluation of ghost images and stray light of the cluster eye [56]. It is furthermore examined which sensitivities and resolution can theoretically be obtained. In the following, the fabrication and experimental characterization of this telescope compound eye imaging system are discussed. The ideal parameters of the finally realized device can be found in [56].

4.2. Fabrication

A cluster eye with 21×3 optical channels was fabricated by micro-optics technology. The microlens shapes are defined by reflow of photoresist cylinders on varying (ellipsoidal) bases. The microlenses are subsequently transferred into fused silica by reactive ion etching. Arrays of apertures with ellipsoidal (focusing array), rectangular (field MLA) and circular openings (relaying MLA) are applied to the corresponding MLAs by chromium etching or lift-off. Finally, the three MLA wafers are stacked in a modified SUSS mask aligner MA8/BA6 with active control of axial distances, wedge error compensation and lateral alignment using appropriate marks. The principle arrangement of the realized cluster eye is given in figure 19.

The major issue of the MLA fabrication by the reflow process is the predetermination of the microlens shape by the resist height and the shape of the lens base within the parameter space used [48]. As experiments showed, the microlens height is approximately constant for a variation of the resist cylinder base within a certain accuracy [55], thus the radius of curvature of the microlens is just given by the size of the lens base.

A critical task in the fabrication was to determine the experimentally obtained radii of curvature and deviations of the cross sections of the ellipsoidal lenses from circles in order to find the best combinations of fabricated samples of all three layers. Thus, after the RIE-transfer of the photoresist profiles into fused silica the MLAs were characterized by a mechanical stylus instrument which was moved on paths crossing all the microlens vertices of the corresponding row or column. Figure 20 demonstrates examples of the measured radii of curvature of the focusing array (ellipsoidal microlenses) in comparison to the ideal values. The deviation of the microlens cross sections from a sphere is always below 90 nm (RMS). The radius error is below 2%.

The best combination of fabricated MLAs taking into account lens fabrication errors was found by implementing the measured microlens data into the ray-tracing and optimization software ZEMAX^{TM} and starting a redesign. The degrees of freedom left to achieve optimum performance are the axial distances between the arrays defined by the glue thicknesses.

Tolerances for lateral and axial alignment of the different substrates when stacking in the SUSS alignment system are better than $\pm 2\ \mu$m and $\pm 2.5\ \mu$m, respectively.

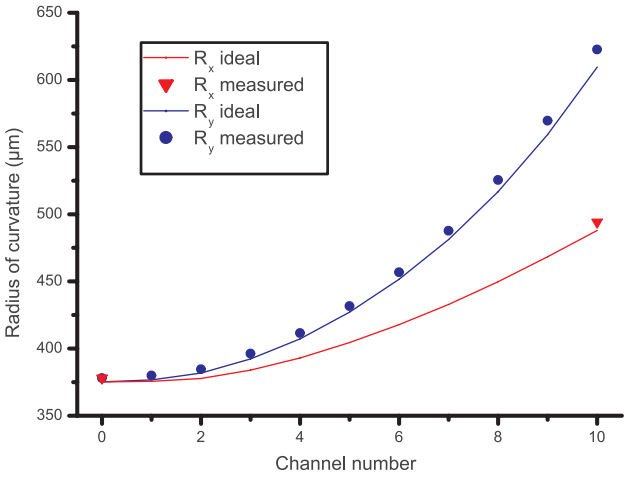

Figure 20. Comparison of ideal and experimentally obtained radii of curvatures of ellipsoidal microlenses of focusing array.

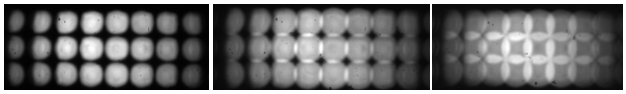

(*a*) (*b*) (*c*)

Figure 21. Image of a white surface. Parts (*a*)–(*c*) show the same image produced by the cluster eye but with different axial positions of the relay optics (distance of 120 μm with respect to each other).

4.3. Experiments

Test patterns were presented to the realized cluster eye and the overall image was relayed onto a conventional CCD camera by a microscope objective with a magnification of 5× and a numerical aperture (NA) of 0.18.

The image annexation of all the partial images can be observed by imaging a white surface, because one smooth white image should be generated. Figure 21 demonstrates that a perfect image stitching could not be obtained with this first demonstrator. Either the partial images are of roughly rectangular shape but do not connect to each other (figure 21(*a*)), or they connect only in some portions (figure 21(*b*)) or have strong overlap in others (figure 21(*c*)). This causes a considerable intensity modulation even for a smooth white object.

Since the cluster eye is non-telecentric on the image side, the chief rays behind the cluster eye are not parallel to the optical axis and possess steeper angles with increasing object size and therefore image coordinate. Due to the limited NA of the relaying microscope objective, the transmitted field angles are restricted and only a limited number of channels can be observed. However, with the central 8 × 3 channels the following images were captured.

Figure 22 shows the images of a radial star pattern, captured at different axial positions from the cluster eye. It can be observed that the matching of the image plane of the individual telescopes with the position of the perfect annexation of the partial images is particularly critical. This is mainly influenced by the correspondence of the axial position

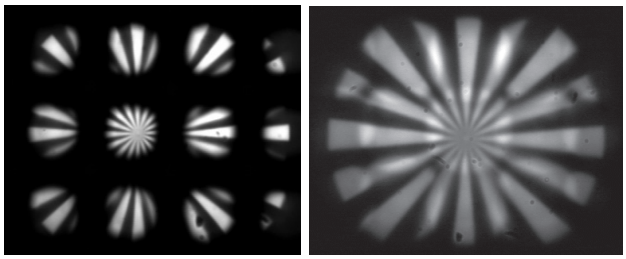

(*a*) (*b*)

Figure 22. Images of a radial star test pattern at an object distance of 41 cm. (Here 5 × 3 channels are contributing.) (*a*) At a certain distance from the cluster eye, the partial images have high contrast but are separated from each other. (*b*) When moving the image plane 120 μm further away from the cluster eye, all the partial images exhibit a very good annexation with only minor areas of overlap or lack of annexation. One regular image is generated by transfer of the different image section through separate channels. However, the contrast of the partial images is reduced compared to (*a*) because the image plane of the telescopes is slightly defocused.

of the intermediate images with the position of the field apertures. The poor quality of the produced field apertures is considered to be less important. Tolerances of MLA fabrication and assembly are very tight (in the μm order of magnitude) and there are no compensation possibilities without reducing either contrast of the partial images or degrading the image stitching. However, it is demonstrated that one overall image is generated by the transfer of different image sections through separated channels with a strong demagnification. Each channel has a FOV of 4.1° × 4.1°, the size of the partial images is 192 × 192 μm^2. This results in a magnification with an equivalent focal length of 2.75 mm at a system length of the realized cluster eye of only 1.99 mm equivalent to a telephoto ratio of 1.4.

In figure 23, images of bar targets of different spatial frequencies are presented. Over a FOV of 33°× 12°, a resolution of 3.3 LP/degree is achieved. Problems of image stitching and aberrations of each channel's marginal field angles can be observed in figures 23(*b*) and (*c*). Bar targets which are oriented parallel to the transition between channels lose modulation in the transition area, while bar targets, which are perpendicular to the direction of transition, are still visible in the transition area. This is the result of a slight offset of the images in the direction of transition between images and the asymmetrical form of the geometrical spots. This is caused by the off-axis aberrations of each channel's marginal fields. Bar targets of different spatial frequencies, such as in figure 23, were imaged for a quantitative MTF determination (figure 24). Each SFR was calculated after the same procedure as discussed for the artificial apposition compound eye. Finally, images of different test patterns visualizing the optical performance of the cluster eye are presented in figure 25. Distant text and faces can be resolved. Due to the non-telecentricity of the cluster eye on the image side (larger chief ray angle for large image coordinate), the relay objective cannot transmit outer portions of the cluster eye image onto the standard imager if the angles are too

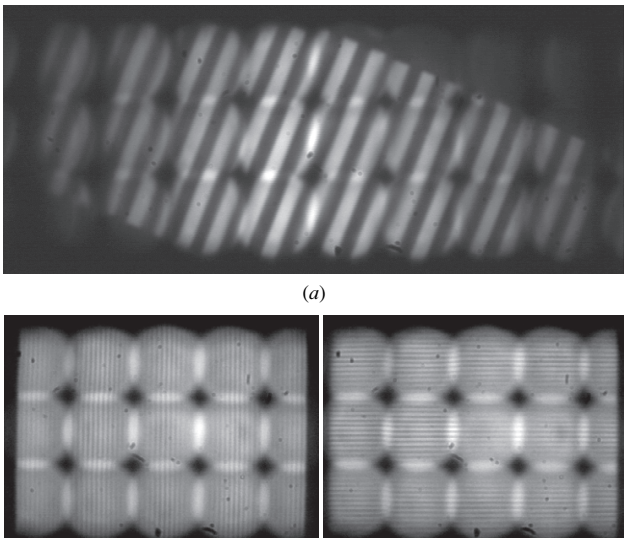

(*a*)

(*b*) (*c*)

Figure 23. Imaged bar targets. (*a*) Tilted bar target with a period of 8.8 mm LP^{-1} and a height of 7 cm at a distance of 55 cm. A good image annexation can be observed, the edges of the bars are imaged sharply. (*b*) Image of vertical test pattern at a distance of 41 cm and size of 13.5 cm, demonstrating the maximum resolution of the cluster eye. (*c*) The same resolution is achieved imaging a horizontal test pattern.

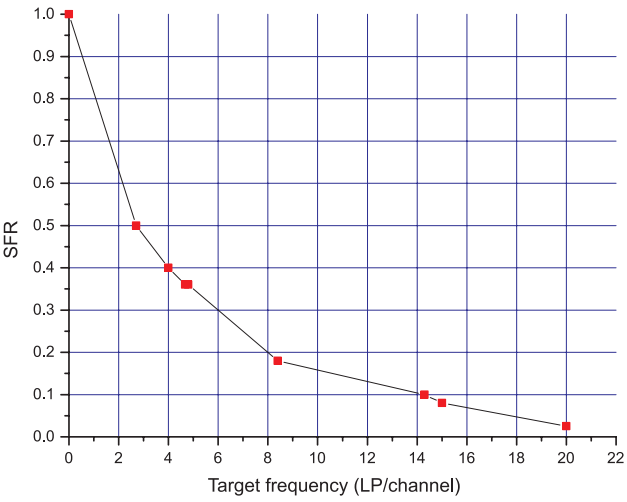

Figure 24. Measured MTF of the fabricated cluster eye.

large (limited numerical aperture of the relay objective). In order to avoid this, a thin ground diffusing glass is introduced in the image plane of the cluster eye so that for large image coordinates the light is also diffused in virtually all angles and thus can be captured by the relay optics. The relayed image becomes more coarse but is still visible (figure 26(*a*)) and larger FOVs can be relayed. The whole image plane of the cluster eye is now relayed using a C-mount objective instead of a microscope objective. The functionality of the cluster eye for objects filling almost all of the design FOV is shown in figure 26(*b*) and (*c*).

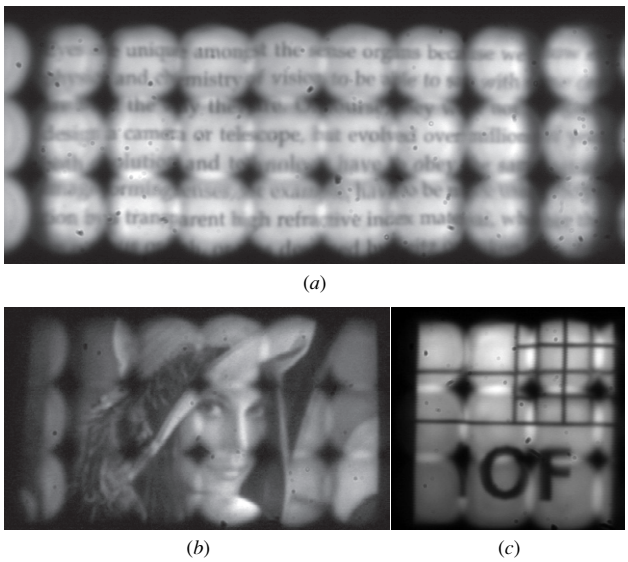

(*a*)

(*b*) (*c*)

Figure 25. Experimental demonstration of the imaging capabilities of the cluster eye. (*a*) Image of a text section of M F Land's book *Animal Eyes*, section 3: 'What makes a good eye' [5] with size 10×3.7 cm^2 at a distance of 17 cm. (*b*) Image of a picture of 'Image processing Lena'. (*c*) Image of the IOF institute logo. Sharp edges and small resolved image features demonstrate the promising imaging capabilities of the cluster eye.

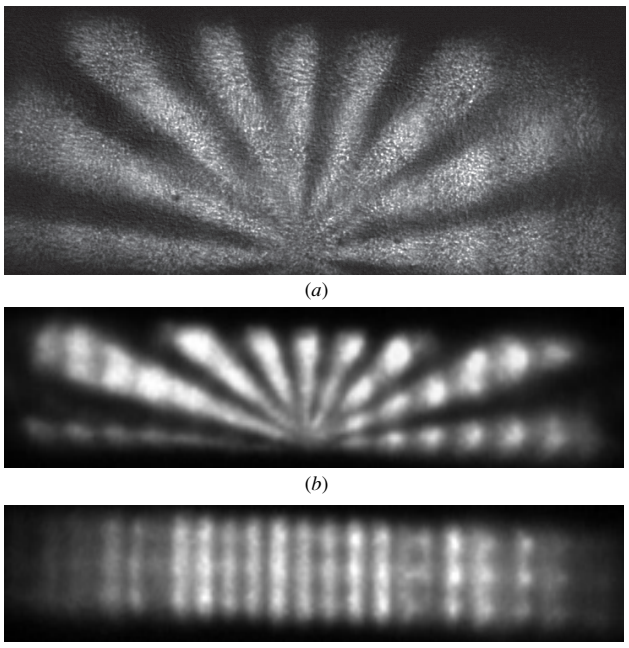

(*a*)

(*b*)

(*c*)

Figure 26. Ground diffusing glass introduced in the image plane of cluster eye. (*a*) Relay by microscope objective (8×3 channels observed, imaging a section of a radial star pattern). (*b*) C-mount objective ($f = 16$ mm, $F/\# = 1.4$, with extension rings) used for relay of the image of a radial star pattern formed by the cluster eye. A horizontal FOV of 63° can be observed. 16×3 channels contribute. (*c*) A bar target with period 3° LP^{-1} is imaged by the cluster eye onto the diffusing glass and relayed by the C-mount objective onto the CCD. 21 LP can be observed resulting in a FOV of 63°. The resolution is degraded for the outer channels.

5. Conclusions and outlook

The technically achieved resolutions of 1.5 LP/degree of the artificial apposition compound eye objective and 3.3 LP/degree for the cluster eye seem rather promising compared to today's standard imaging devices, if the difference in system length of approximately one order of magnitude is taken into account. For comparison, a classical single aperture wide-angle objective with a 70° horizontal field of view and a '1 megapixel' sensor provides an angular resolution of 7.1 LP/degree if homogeneous resolution over the field of view is assumed. The total track of such a 'miniature' single aperture objective is typically in the order of magnitude of 5–10 mm. The angular resolution of the demonstrated artificial apposition compound eyes is furthermore comparable to that of many invertebrate eyes such as, e.g., the honeybee (0.5 LP/degree). The natural archetypes show that it is not the highest resolution that provides the optical solution capable of surviving for millions of years, but the simplest solution in perfect adaptation to the image capturing task and to the environmental circumstances such as minimum volume, no need for focusing for different object distances and minimum necessary signal processing.

In the future, modifications of the technology have to be developed for the FOV and resolution of artificial compound eye imaging systems to be increased, the expensive lithographical process to be replaced by cheap replication, objectives to become mechanically flexible or be directly integrated in the electronics fabrication process. Additional functions which are also provided by the natural archetypes such as color vision, polarization sensitivity and movement detection shall be integrated as well. The combination of micro-optical imaging systems with task-specific image processing such as artificial neural networks, which also could be inspired by insect vision, must be investigated.

Finally, comparing the analyzed artificial compound eye concepts with their natural archetypes the following conclusions can be drawn. The major difference at this stage of development is the planar arrangement of the artificial systems compared to the curved geometry of the natural ones. This is the consequence of today's limitation of planar lithographic patterning technologies. The advantages of a curved base compared to a planar one are obvious: the immanence of a large field of view, avoiding off-axis aberrations, and avoiding declining illumination with increasing field angle due to the $\cos^4$ law. Technologies to generate microlens arrays on curved surfaces, e.g. by a special type of a laser beam writer, are currently being developed. Optoelectronics on curved surfaces have to be investigated in future.

However, artificial compound eye imaging systems, in addition to the compactness and large telephoto ratio, exhibit one major advantage for solving the problem of off-axis aberrations: because of the segmented image transfer each channel can be specially optimized for its individual viewing direction resulting in a drastically improved resolution homogeneity over the objectives' entire FOV while classical single-channel imaging systems always have to be a compromise for all the angles of incidence represented in the FOV.

Acknowledgments

We would like to acknowledge the contributions of Peter Dannberg from the Fraunhofer Institute of Applied Optics and Precision Engineering (IOF), Jena, who is responsible for the fabrication of the different types of artificial apposition compound eye objectives using micro-optics technology. His exceptionally good aligned UV-replication of microlens arrays is the key of the successful fabrication of the presented demonstrators. The previous work of, and the countless discussions with, Reinhard Völkel from SUSS MicroOptics SA (Neuchâtel, Switzerland) gave us much inspiration for our work on unorthodox, bioinspired imaging principles. The experience of Martin Eisner (also SUSS MicroOptics) in the aligned stacking of microlens array wafers finally lead to the realization of the cluster eye. We are furthermore very thankful for the help we got from our colleagues from the Institute of Microtechnology (IMT) of the University of Neuchâtel, Switzerland, especially Toralf Scharf who took very important steps in the fabrication of the lens and aperture arrays of the cluster eye. We would also like to acknowledge Pierre-Francois Rüedi and Pascal Nussbaum from the Centre Swiss d'Electronique et de Microtechnique SA (CSEM) Neuchâtel, Switzerland, for the distribution of the artificial retina CMOS sensor array, which we combined with the artificial apposition compound eye objectives and connected to digital cameras.

References

[1] Lohmann A W 1989 Scaling laws for lens systems *Appl. Opt.* **28** 4996–8
[2] Völkel R, Eisner M and Weible K J 2003 Miniaturized imaging systems *Microelectron. Eng.* **67–68** 461–72
[3] Sanders J S (ed) 1996 *Selected Papers on Natural and Artificial Compound Eye Sensors (SPIE Milestone Series)* 122nd edn (Bellingham, WA: SPIE)
[4] Hutley M C, Hunt R, Stevens R F and Savander P 1994 The Moiré magnifier *Pure Appl. Opt.* **3** 133–42
[5] Land M F and Nilsson D-E 2002 *Animal Eyes (Oxford Animal Biology Series)* (Oxford: Oxford University Press)
[6] Land M F 1988 The optics of animal eyes *Contemp. Phys.* **29** 435–55
[7] Exner S 1891 *Die Physiologie der Facettierten Augen von Krebsen und Insecten* (Leipzig: Deuticke)
[8] Land M F 1978 Animal eyes with mirror optics *Sci. Am.* **239** 126–134
[9] Land M F 2000 Eyes with mirror optics *Pure Appl. Opt.* **2** R44–R50
[10] Snyder A W, Stavenga D G and Laughlin S B 1977 Spatial information capacity of compound eyes *J. Comp. Physiol.* A **116** 183–207
[11] Goetz K G 1965 Die optischen uebertragungseigenschaften der komplexaugen von drosophila *Kybernetik* **2** 215–21
[12] Land M F 1980 Compound eyes: old and new optical mechanisms *Nature* **287** 681–6
[13] Hecht E 1989 *Optik* 3rd edn (Reading, MA: Addison-Wesley)
[14] Snyder A W 1977 Physics of vision in compound eyes *Handbook of Sensory Physiology* (Berlin: Springer) pp 225–313
[15] Horridge G A 1978 The separation of visual axes in apposition compound eyes *Phil. Trans. R. Soc.* B **285** 1–59
[16] Barlow H B 1952 The size of ommatidia in apposition eyes *J. Exp. Biol.* **29** 667–74

[17] Kirschfeld K 1976 The resolution of lens and compound eyes *Neural Principles in Vision* (Berlin: Springer) pp 354–70
[18] Horridge G A 1977 The compound eye of insects *Sci. Am.* **237** 108–20
[19] Land M F 1989 Variations in structure and design of compound eyes *Facets of Vision* ed D Stavenga and R C Hardie (Berlin: Springer) chapter 5, pp 90–111
[20] Sanders J S and Halford C E 1995 Design and analysis of apposition compound eye optical sensors *Opt. Eng.* **34** 222–35
[21] Hamanaka K and Koshi H 1996 An artificial compound eye using a microlens array and its application to scale-invariant processing *Opt. Rev.* **3** 264–8
[22] Ogata S, Ishida J and Sasano T 1994 Optical sensor array in an artificial compound eye *Opt. Eng.* **33** 3649–55
[23] Hoshino K, Mura F and Shimoyama I 2001 A one-chip scanning retina with an integrated micromechanical scanning actuator *J. Microelectromech. Syst.* **10** 492–7
[24] Franceschini N, Pichon J M and Blanes C 1992 From insect vision to robot vision *Phil. Trans. R. Soc.* B **337** 283–94
[25] Tanida J, Kumagai T, Yamada K and Miyatake S 2001 Thin observation module by bound optics (TOMBO) concept and experimental verification *Appl. Opt.* **40** 1806–13
[26] Kitamura Y *et al* 2004 Reconstruction of a high-resolution image on a compound-eye image-capturing system *Appl. Opt.* **43** 1719–27
[27] Lee L P and Szema R 2005 Inspirations from biological optics for advanced photonic systems *Science* **310** 1148–50
[28] Jeong K, Kim J and Lee L P 2005 Polymeric synthesis of biomimetic artificial compound eyes *Transducers '05: Proc. 13th Int. Conf. on Solid-State Sensors, Actuators and Microsystems* pp 1110–4
[29] McIntyre P and Caveney S 1985 Graded index optics are matched to optical geometry in the superposition eyes of scarab beetles *Phil. Trans. R. Soc.* B **311** 237–69
[30] Land M F, Burton F and Meyer-Rochow V 1979 The optical geometry of euphausiid eyes *J. Comp. Physiol.* A **130** 49–62
[31] Navarro R and Franceschini N 1998 On image quality of microlens arrays in diurnal superposition eyes *Pure Appl. Opt.* **7** 69–78
[32] Gabor D 1940 Improvements in or relating to optical systems composed of lenticules *Patent UK* 541,753
[33] Hutley M, Stevens R F and Hembd C 1997 Imaging properties of the 'Gabor superlens' *Digest of Top. Meet. on Microlens Arrays at NPL, Teddington* vol 13 ed M C Hutley (EOS) pp 101–4
[34] Hutley M C 1993 Integral photography, superlenses and the Moiré magnifier *Digest of Top. Meet. on Microlens Arrays at NPL, Teddington* vol 2 ed M C Hutley (EOS) pp 72–5
[35] Kawazu M and Ogura Y 1980 Application of gradient-index fiber arrays to copying machines *Appl. Opt.* **19** 1105–12
[36] Borrelli N F, Bellman R H, Durbin J A and Lama W 1991 Imaging and radiometric properties of microlens arrays *Appl. Opt.* **30** 3633–42
[37] Hugle W B, Daendliker R and Herzig H P 1993 Lens array photolithography *Patent US* 8,114,732
[38] Duparré J, Dannberg P, Schreiber P, Bräuer A and Tünnermann A 2004 Artificial apposition compound eye fabricated by micro-optics technology *Appl. Opt.* **43** 4303–10
[39] Duparré J, Dannberg P, Schreiber P, Bräuer A, Nussbaum P, Heitger F and Tünnermann A 2004 Ultra-thin camera based on artificial apposition compound eyes *Proc. 10th Microopt. Conf.* ed W Karthe, G D Khoe and Y Kokubun (Amsterdam: Elsevier)
[40] Stevens R F 1999 Optical inspection of periodic structures using lens arrays and Moiré magnification *Imaging Sci. J.* **47** 173–9
[41] Kamal H, Völkel R and Alda J 1998 Properties of Moiré magnifiers *Opt. Eng.* **37** 3007–14
[42] Snyder A W 1977 Acuity of compound eyes: physical limitations and design *J. Comp. Physiol.* A **116** 161–82
[43] Hessler T, Rossi M, Pedersen J, Gale M T, Wegner M and Tiziani H J 1997 Microlens arrays with spatial variation of the optical functions *Digest of Top. Meet. on Microlens Arrays at NPL, Teddington* vol 13 ed M C Hutley (EOS) pp 42–7
[44] Sinzinger S and Jahns J 1997 Integrated micro-optical imaging system with a high interconnection capacity fabricated in planar optics *Appl. Opt.* **36** 4729–35
[45] Dannberg P, Mann G, Wagner L and Bräuer A 2000 Polymer UV-molding for micro-optical systems and O/E-integration *Proc. of Micromachining for Micro-Optics* vol 4179 ed S H Lee and E G Johnson (Bellingham, WA: SPIE) pp 137–45
[46] Popovich Z D, Sprague R A and Conell G A N 1988 Technique for monolithic fabrication of microlens arrays *Appl. Opt.* **27** 1281–4
[47] Vökel R, Herzig H P, Nussbaum P and Dändliker R 1996 Microlens array imaging system for photolithography *Opt. Eng.* **35** 3323–30
[48] Lindlein N, Haselbeck S and Schwider J 1995 Simplified theory for ellipsoidal melted microlenses *Digest of Top. Meet. on Microlens Arrays at NPL, Teddington* vol 5 ed M C Hutley (EOS) pp 7–10
[49] Wippermann F, Duparré J, Schreiber P and Dannberg P 2005 Design and fabrication of a chirped array of refractive ellipsoidal micro-lenses for an apposition eye camera objective *Proc. of Optical Design and Engineering II* ed L Mazuray and R Wartmann (Bellingham, WA: SPIE) pp 5962, 59 622C-1-59 622C-11
[50] Rüedi P-F, Heim P, Kaess F, Grenet E, Heitger F, Burgi P-Y, Gyger S and Nussbaum P 2003 A 128 x 128 pixel 120-dB dynamic-range vision-sensor chip for image contrast and orientation extraction *IEEE J. Solid-State Circ.* **38** 2325–33
[51] Duparré J, Dannberg P, Schreiber P, Bräuer A and Tünnermann A 2005 Thin compound eye camera *Appl. Opt.* **44** 2949–56
[52] Duparré J, Wippermann F, Dannberg P and Reimann A 2005 Chirped arrays of refractive ellipsoidal microlenses for aberration correction under oblique incidence *Opt. Exp.* **13** 10539–51
[53] Vökel R and Wallstab S 1999 Flachbauendes Bilderfassungssystem *Patent* DE 199 17 890A1
[54] Duparré J, Schreiber P and Vökel R 2003 Theoretical analysis of an artificial superposition compound eye for application in ultra flat digital image acquisition devices *Proc. of Optical Design and Engineering* vol 5249 ed L Mazurany, P J Rogers and R Wartmann (Bellingham, WA: SPIE) pp 408–18
[55] Duparré J, Schreiber P, Dannberg P, Scharf T, Pelli P, Vökel R, Herzig H-P and Bräuer A 2004 Artificial compound eyes-different concepts and their application to ultra flat image acquisition sensors *Proc. of MOEMS and Miniaturized Systems IV* vol 5346 ed A El-Fatatry (Bellingham, WA: SPIE) pp 89–100
[56] Duparré J, Schreiber P, Matthes A, Pshenay-Severin E, Bräuer A, Tünnermann A, Vökel R, Eisner M and Scharf T 2005 Microoptical telescope compound eye *Opt. Exp.* **13** 889–903